Avoiding Dynamic Singularities in Cartesian Motions of Free-Floating Manipulators

KOSTAS NANOS
EVANGELOS PAPADOPOULOS, Senior Member, IEEE
National Technical University of Athens
Athens, Greece

Free-floating manipulators are subject to dynamic singularities that complicate their Cartesian motions and restrict their workspace. In this work, the Cartesian trajectory planning of free-floating manipulators is studied. A methodology is developed in which, for given end-effector trajectories, appropriate initial system configurations are found that result in singularity avoidance during end-effector motion. The method applies to both planar and spatial systems, with and without initial angular momentum, and to any desired end-effector position and attitude trajectories.

Manuscript received April 28, 2014; revised October 17, 2014; released for publication February 21, 2015.

DOI. No. 10.1109/TAES.2015.140343.

Refereeing of this contribution was handled by S. Karaman.

Authors' address: National Technical University of Athens, Mechanical Engineering, Heroon Polytechniou 9, Athens 15780, Greece, E-mail: (egpapado@central.ntua.gr).

I. INTRODUCTION

Robots in space are playing important roles in planetary exploration and in tasks on orbit, due to their ability to execute tasks impossible to humans and to act in inaccessible or too-risky environments. On-orbit robotic systems consist of an on-orbit, thruster-equipped spacecraft (base) fitted with one or more robotic manipulators (see Fig. 1). Examples of such systems include the ETS-VII [1] and the Orbital Express [2].

To conserve fuel or avoid interactions with nearby objects, all spacecraft actuators may be turned off. Then the system operates in a free-floating mode during which the spacecraft translates and rotates in response to manipulator motions due to the dynamic coupling between the spacecraft and its manipulator. This mode of operation is feasible when no external forces or torques act on the system. In general during operations, zero angular momentum is desired. However, small amounts of angular momentum may be present due to previous on/off thruster action or to collisions with the environment. Moreover, the effective Cartesian space motion of such systems is subject to the existence of dynamic singularities (DSs) [3]. These are due to the dependence of the end-effector velocity on both manipulator and spacecraft motions, and unlike the singularities of fixed-base manipulators, they are functions of the dynamic properties of the system. At DSs, the manipulator is unable to move its end-effector in some inertial direction, while their location in the workspace is path dependent due to the nonholonomic nature of the Cartesian motion; hence the DSs must be considered in the design, planning, and control of free-floating manipulator systems.

Over the past decades, the dynamics, planning, and control of space manipulators have been studied by a number of researchers [4]. The planning and control of an underactuated free-floating space system is complicated due to the nonintegrability of the system's angular momentum [5]. To describe the system's kinematics, the Virtual Manipulator approach developed by Vafa and Dubowsky [6] can be used in modeling, path planning, and workspace analysis of such systems. Papadopoulos and Dubowsky [7] showed that nearly any terrestrial fixed-base control algorithm can be applied to space manipulators if a few additional conditions hold. They also showed [3] that the free-floating manipulators exhibit DSs which cannot be predicted by the kinematic properties of the system and whose location in the workspace is path dependent.

The system's reachable workspace, a qualitative and quantitative analysis of which is presented in [8], is restricted by the presence of a DS. Umetani and Yoshida [9] introduced the free-floating system generalized Jacobian and developed a resolved motion-rate control method based on it. However, the method fails in the presence of a DS. Caccavale and Siciliano [10] employed the generalized Jacobian in solving the inverse kinematics of a free-floating space manipulator. The flatness theory has been used in planning trajectories for free-floating

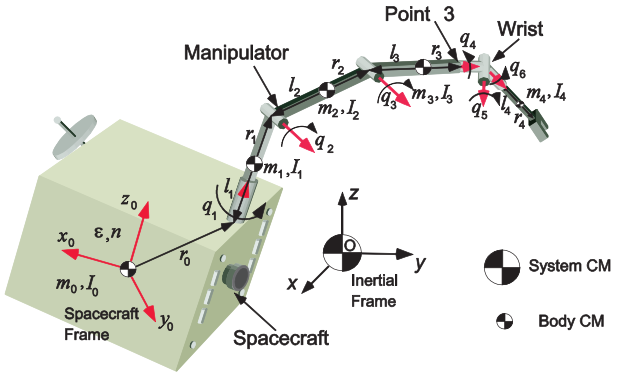

Fig. 1. Spatial free-floating space robot and definition of its parameters.

systems [11–12]. The method requires the selection of particular parameters so that the system is made controllable and linearizable by prolongations.

Papadopoulos [5] has presented a point-to-point Cartesian-space planning method that permits the effective use of a system's reachable workspace avoiding DS; no attempt to follow a predefined path was made. Tortopidis and Papadopoulos [13] developed a point-to-point, polynomial-function-based path-planning method that allows for endpoint location and simultaneous spacecraft attitude control using manipulator actuators only. Since the proposed method was applied in joint space, it was immune to DS. Pandey and Agrawal [14] addressed the problem of path planning for a free-floating prismatic manipulator; however, only a final end-effector position and orientation—not a path—are defined. Lampariello et al. [15] applied a motion-planning method for free-flying manipulators which yields optimal solutions for spacecraft actuation and motion duration, avoiding unnecessary spacecraft actuation. However, to avoid the appearance of DSs, motion planning is done in the joint space rather than in the task space, where tasks are defined.

A method for grasping and stabilizing a noncooperative free-floating target satellite is proposed in [16]. The method includes a path-tracking phase, in which singularities are avoided indirectly through a cost-function minimization. Xu et al. [17] have proposed a trajectory-planning method using damped least squares to avoid a DS by deviating the end-effector from its desired path. However, both methods require manipulator redundancy. Dimitrov and Yoshida [18] introduced a holonomic distribution control concept to plan reactionless Cartesian end-effector paths. Redundant manipulators were used and no end-effector path was defined. Wang and Xie [19] have developed an adaptive Jacobian tracking control system for free-floating manipulators with uncertain kinematic and dynamic properties; however, to apply this controller, the end-effector is assumed to be outside the workspace area where singularities may appear.

Many research works deal with the capturing of tumbling satellites by space robots where momentum exchange appears. Distributed momentum control has been proposed [20–23] so that the spacecraft attitude reactions during the approach and postimpact phases are minimized. Several time-optimal control methods have been presented [24–27], considering either the constraints on the reaction wheel torques or the momentum it can store, along with the constraints on the grasping forces and torques. In all these works, the spacecraft attitude is controlled with the reaction wheel. An adaptive control algorithm has been proposed so that the derived manipulator motions result in minimum disturbance to the spacecraft following the capture of an unknown tumbling target [28]. The proposed algorithm was applied in joint space on redundant manipulators, and thus was immune to DS.

Although zero initial system angular momentum is desired before a robot motion, small amounts of angular momentum may be present, as mentioned earlier. Matsuno and Saito [29] presented an attitude point-to-point control law of a planar two-link space robot with angular momentum, which takes the system to the desired location. However, the system drifts away due to the angular momentum. To effectively utilize the angular momentum generated by momentum wheels, Yamada et al. [30] proposed a path-planning method for an arm on a free-floating satellite. However, no desired end-effector path was defined. The kinematics and momentum equations of space manipulators were presented by Nenchev et al. [31]. They focused on the redundant nature of free-flying systems and proposed a least-squares approach to resolve system redundancy. The solutions were applied on tasks with zero system momentum.

To avoid DSs, all previous research works have used either manipulator redundancy or point-to-point path-planning techniques. However, the redundancy complicates system design, while many space tasks demand exact end-effector path following. In our previous work [32], we have introduced a preliminary technique which permits straight-line planning only of a nonredundant free-floating space manipulator avoiding DS when its angular momentum is zero. Here this technique is developed into a method allowing motion along any end-effector path, which may lie in the entire workspace, including the path-dependent workspace. Moreover, the system is allowed to have nonzero angular momentum. It is shown not only that the presence of angular momentum affects the value of the initial spacecraft attitude but also that this attitude depends on the duration of the end-effector motion. Also, the method is applicable to both planar and spatial systems allowing commands for both end-effector desired position and orientation. The application of the method is illustrated by two examples.

II. DYNAMICS OF FREE-FLOATING SPACE MANIPULATORS

A space manipulator system consists of a spacecraft and a manipulator mounted on it. When the system is

operating in free-floating mode, the spacecraft attitude-control system is turned off. In this mode, no external forces and torques act on the system, and hence the spacecraft translates and rotates in response to manipulator motions.

We consider a system whose manipulator has revolute joints and an anthropomorphic open-chain kinematic configuration for maximum reachable workspace. In a system with a manipulator that has N degrees of freedom (dof), there will be $N + 6$ dof in total, including the spacecraft dof. The assumption of zero external forces and initial linear momentum results in a fixed system center of mass, which can then coincide with the origin O of the inertial coordinate frame (see Fig. 1). The initial angular momentum of the system is not assumed to be zero.

In the absence of external torques, the system angular momentum is conserved. The conservation equation is then

$$ {}^{0}\mathbf{D}\,(\mathbf{q})\,{}^{0}\boldsymbol{\omega}_{\mathbf{0}} + {}^{0}\mathbf{D}_{\mathbf{q}}\,(\mathbf{q})\,\dot{\mathbf{q}} = \mathbf{R}_{\mathbf{0}}^{\mathbf{T}}\,(\boldsymbol{\varepsilon}, n)\,\mathbf{h}_{\mathbf{CM}}, \tag{1} $$

where ${}^{0}\boldsymbol{\omega}_{\mathbf{0}}$ is the spacecraft angular velocity expressed in the spacecraft zeroth frame, the $N \times 1$ column vectors $\mathbf{q}$ and $\dot{\mathbf{q}}$ represent manipulator joint angles and rates, respectively, and ${}^{0}\mathbf{D}$ and ${}^{0}\mathbf{D}_{\mathbf{q}}$ are inertia-type matrices of appropriate dimensions, given in [3]. The matrix $\mathbf{R}_{\mathbf{0}}(\boldsymbol{\varepsilon}, n)$ is the rotation matrix between the spacecraft zeroth frame and the inertial frame expressed as a function of the spacecraft unit quaternion $\boldsymbol{\varepsilon}$, n, and $\mathbf{h}_{\mathbf{CM}}$ is the system angular momentum expressed in the inertial frame.

The vector $\mathbf{v}_{\mathbf{E}}$ contains the end-effector linear velocity $\dot{\mathbf{r}}_{\mathbf{E}}$ and angular velocity $\boldsymbol{\omega}_{\mathbf{E}}$ and is given by

$$ \mathbf{v}_{\mathbf{E}} = \begin{bmatrix} \dot{\mathbf{r}}_{\mathbf{E}} \\ \boldsymbol{\omega}_{\mathbf{E}} \end{bmatrix} = \mathbf{C}\,(\boldsymbol{\varepsilon}, n) \begin{bmatrix} {}^{0}\mathbf{J}_{\mathbf{11}}^{*} & {}^{0}\mathbf{J}_{\mathbf{12}}^{*} \end{bmatrix} \begin{bmatrix} {}^{0}\boldsymbol{\omega}_{\mathbf{0}} \\ \dot{\mathbf{q}} \end{bmatrix}, \tag{2} $$

where

$$ \mathbf{C}\,(\boldsymbol{\varepsilon}, n) = \begin{bmatrix} \mathbf{R}_{\mathbf{0}}\,(\boldsymbol{\varepsilon}, n) & \mathbf{0}_{\mathbf{3x3}} \\ \mathbf{0}_{\mathbf{3x3}} & \mathbf{R}_{\mathbf{0}}\,(\boldsymbol{\varepsilon}, n) \end{bmatrix} \tag{3a} $$

and

$$ {}^{0}\mathbf{J}_{\mathbf{11}}^{*} = \begin{bmatrix} {}^{0}\mathbf{J}_{\mathbf{11}}^{\mathrm{T}} & \mathbf{I} \end{bmatrix}^{\mathrm{T}} \tag{3b} $$

$$ {}^{0}\mathbf{J}_{\mathbf{12}}^{*} = \begin{bmatrix} {}^{0}\mathbf{J}_{\mathbf{12}}^{\mathrm{T}} & {}^{0}\mathbf{J}_{\mathbf{22}}^{\mathrm{T}} \end{bmatrix}^{\mathrm{T}}. \tag{3c} $$

The ${}^{0}\mathbf{J}_{\mathbf{11}}$, ${}^{0}\mathbf{J}_{\mathbf{12}}$, and ${}^{0}\mathbf{J}_{\mathbf{22}}$ terms are functions of $\mathbf{q}$ and are given in detail in [3], and $\mathbf{I}$ is the 3×3 unity matrix.

III. TRAJECTORY PLANNING AND DYNAMIC SINGULARITIES

In this section, we focus on the Cartesian-space trajectory planning of a spatial free-floating manipulator whose end-effector has to follow a desired path in prescribed time. The path is defined by $\mathbf{v}_{\mathbf{E}}(\mathrm{t})$. During system motion, the conservation of angular momentum, given by (1), must be satisfied. Combining (1) and (2) in matrix form results in the following equation:

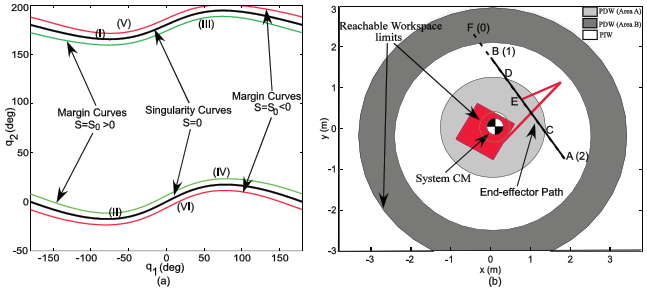

Fig. 2. (a) Singularity and margin curves in joint space. (b) PIW and PDW areas for 2-dof planar space robot. At E, manipulator may become singular.

$$ \mathbf{A} \begin{bmatrix} {}^{0}\boldsymbol{\omega}_{\mathbf{0}} \\ \dot{\mathbf{q}} \end{bmatrix} = \begin{bmatrix} \mathbf{R}_{\mathbf{0}}^{\mathbf{T}} & \mathbf{0}_{\mathbf{3x6}} \\ \mathbf{0}_{\mathbf{6x3}} & \mathbf{C}^{\mathbf{T}} \end{bmatrix} \begin{bmatrix} \mathbf{h}_{\mathbf{CM}} \\ \mathbf{v}_{\mathbf{E}} \end{bmatrix}, \tag{4} $$

where the $9 \times (N+3)$ matrix $\mathbf{A}$ is given by

$$ \mathbf{A} = \begin{bmatrix} {}^{0}\mathbf{D} & {}^{0}\mathbf{D}_{\mathbf{q}} \\ {}^{0}\mathbf{J}_{\mathbf{11}}^{*} & {}^{0}\mathbf{J}_{\mathbf{12}}^{*} \end{bmatrix}_{9\times(N+3)}. \tag{5} $$

Given $\mathbf{v}_{\mathbf{E}}(\mathrm{t})$ and $\mathbf{h}_{\mathbf{CM}}$, (4) yields the required joint rates and the spacecraft angular velocity. Equation (4) has at least one solution, if $N \geq 6$. Therefore, the minimum number of manipulator joints of a spatial system, for a given end-effector trajectory $\mathbf{v}_{\mathbf{E}}(\mathrm{t})$, is six. Note that in planar systems, this number reduces to three. In the remainder of this paper, we take $N = 3$ in the planar case and $N = 6$ in the spatial one.

When $N = 6$, (4) has only one solution, if $\det(\mathbf{A}) \neq 0$. Since the matrix ${}^{0}\mathbf{D}$ is invertible, using block matrix properties the following is true:

$$ \begin{aligned} \det(\mathbf{A}) = \det\left({}^{0}\mathbf{D}\right) \det\left(\mathbf{S}^{*}(\mathbf{q})\right) \neq 0 \Rightarrow \\ \det\left(\mathbf{S}^{*}(\mathbf{q})\right) = S(\mathbf{q}) \neq 0, \end{aligned} \tag{6} $$

where $\mathbf{S}^{*}$, called the generalized Jacobian [9], is given by

$$ \mathbf{S}^{*}(\mathbf{q}) = -{}^{0}\mathbf{J}_{\mathbf{11}}^{*}\,{}^{0}\mathbf{D}^{-1}\,{}^{0}\mathbf{D}_{\mathbf{q}} + {}^{0}\mathbf{J}_{\mathbf{12}}^{*}. \tag{7} $$

When $S = 0$, (6) defines the DSs in the joint space and then $\mathbf{A}$ loses its full rank. Due to the DSs, the manipulator reachable workspace is divided in two regions. In the first, called the path-independent workspace (PIW), no dynamic singularities can occur, while in the second, called the path-dependent workspace (PDW), the manipulator may become singular depending on the end-effector path taken to reach a point [3].

In the joint space, $\det(\mathbf{S}^{*}) = \mathrm{S}_0 = \text{const.}$ in (6) defines surfaces (spatial systems) or curves (planar systems). If $\mathrm{S}_0 = 0$, these will be called here singularity surfaces (for spatial systems) or singularity curves (for planar systems); and if $\mathrm{S}_0 \neq 0$, they will be called margin surfaces (for spatial systems) or margin curves (for planar systems). The singularity and margin curves for a 2-dof planar system are shown in Fig. 2a. The singularity curve I in Fig. 2a corresponds to manipulator DS occurring in the

PDW A area, while curve II corresponds to manipulator DS in the PDW B area (see Fig. 2b).

If (6) is satisfied, the spacecraft angular velocity as the end-effector moves, expressed in the spacecraft zeroth frame, is

$$ {}^{\mathbf{0}}\boldsymbol{\omega}_{\mathbf{0}} = \left[{}^{\mathbf{0}}\mathbf{D}^{-1} + {}^{\mathbf{0}}\mathbf{D}^{-1}\,{}^{\mathbf{0}}\mathbf{D}_{\mathbf{q}}\mathbf{S}^{*-1}\,{}^{\mathbf{0}}\mathbf{J}_{\mathbf{11}}^{*}\,{}^{\mathbf{0}}\mathbf{D}^{-1}\right]\mathbf{R}_{\mathbf{0}}^{\mathrm{T}}\mathbf{h}_{\mathbf{CM}} - {}^{\mathbf{0}}\mathbf{D}^{-1}\,{}^{\mathbf{0}}\mathbf{D}_{\mathbf{q}}\mathbf{S}^{*-1}\mathbf{C}^{\mathrm{T}}\mathbf{v}_{\mathbf{E}}, \tag{8a} $$

while the column vector of the joint rates is

$$ \dot{\mathbf{q}} = -\mathbf{S}^{*-1}\,{}^{\mathbf{0}}\mathbf{J}_{\mathbf{11}}^{*}\,{}^{\mathbf{0}}\mathbf{D}^{-1}\mathbf{R}_{\mathbf{0}}^{\mathrm{T}}\mathbf{h}_{\mathbf{CM}} + \mathbf{S}^{*-1}\mathbf{C}^{\mathrm{T}}\mathbf{v}_{\mathbf{E}}. \tag{8b} $$

As shown by (8), the joint rates and the spacecraft angular velocity are proportional to the initial angular momentum and the end-effector linear and angular velocity. The matrices $\mathbf{R_0}(\boldsymbol{\varepsilon}, n)$ and $\mathbf{C}(\boldsymbol{\varepsilon}, n)$ in (8a) and (8b) must be updated using the equations

$$ \begin{bmatrix} \dot{\boldsymbol{\varepsilon}} \\ \dot{n} \end{bmatrix} = \begin{bmatrix} (1/2)\left(\boldsymbol{\varepsilon}^{\times} + n\mathbf{I}\right) \\ -(1/2)\,\boldsymbol{\varepsilon}^{\mathrm{T}} \end{bmatrix} {}^{\mathbf{0}}\boldsymbol{\omega}_{\mathbf{0}}. \tag{8c} $$

Note that if the end-effector is driven from some point A to point B along path AB, and then the motion is reversed so that the end-effector is driven back to point A along the same path and with the same trajectory and time duration but opposite angular momentum, then it will reach A with exactly the same configuration with which it started (see Appendix A). Note that this reverse motion is virtual, i.e., it is not performed by the manipulator during the actual motion. However, it allows the computation of a feasible initial spacecraft attitude using a known spacecraft attitude corresponding to an end-effector location along the desired path. This property will be employed in the methodology developed here.

Equation (8) can be solved numerically to yield the required joint angles $\mathbf{q}$ and the resulting spacecraft attitude $\boldsymbol{\varepsilon}$, n, so that the end-effector follows the desired path with desired attitude. However, these fail in the presence of a DS. One method to avoid DSs is to restrict the end-effector motions in the PIW, thus reducing the system workspace. Next we propose a methodology which allows end-effector path planning that avoids the DS in the PDW and results in an effective use of the entire system workspace.

IV. AVOIDANCE OF DYNAMIC SINGULARITIES

In this section, we introduce the basic analysis leading to DS avoidance, along with the definitions employed in the development of the planning method.

As mentioned in Section III, DS avoidance is achieved if (6) is satisfied during end-effector motion. The function S, given in (6), can take positive or negative values. The satisfaction of (6) can be possible if, during the desired end-effector motion, S does not become zero, i.e., if during the motion its minimum value is $S_{\min} > 0$ (if $S > 0$) or its maximum value is $S_{\max} < 0$ (if $S < 0$). Note that when S takes values close to 0—i.e., near a DS—the manipulator's motion may result in large values of accelerations and torques. Therefore, values of S close to 0 also are undesirable; DS avoidance then requires that $S_{\min} > \mathrm{S}_0 > 0$ or $S_{\max} < \mathrm{S}_0 < 0$, where S_0 a constant. In this section, and without loss of generality, we focus on deriving the minimum values of the function S. The same approach is also applicable if maximum values of S are considered.

As shown in (6), the value of S depends on manipulator configuration $\mathbf{q}$. Since $\mathbf{q}$ is the solution of (8), it is a function of the time t and the initial conditions $\boldsymbol{\varepsilon}_{\mathbf{in}}$, n_{in}, $\mathbf{q}_{\mathbf{in}}$—i.e., $\mathbf{q}(t; \boldsymbol{\varepsilon}_{\mathbf{in}}, n_{\mathrm{in}}, \mathbf{q}_{\mathbf{in}})$. First, we show that $S_{\min}$ is a continuous function of the initial spacecraft attitude, a property that will be used in the next section.

For a given Cartesian path, $\mathbf{q}$ results from the integration of (8), which is of the form $\dot{\mathbf{x}} = \mathbf{f}(t; \mathbf{x}), \mathbf{x} = [\mathbf{q}, \boldsymbol{\varepsilon}, n]^{\mathrm{T}}$. Since $\mathbf{f}$ is composed of trigonometric functions, it is continuous, and in addition, all its partial derivatives are continuous. Thus it can be shown that the solution $\mathbf{x}$ is continuous in t and $\boldsymbol{\varepsilon}_{\mathbf{in}}$, n_{in}, $\mathbf{q}_{\mathbf{in}}$ [33]. Therefore, S is a continuous function of t, $\boldsymbol{\varepsilon}_{\mathbf{in}}$, n_{in}, $\mathbf{q}_{\mathbf{in}}$:

$$ S = S\left(t; \boldsymbol{\varepsilon}_{\mathbf{in}}, n_{\mathrm{in}}, \mathbf{q}_{\mathbf{in}}\right). \tag{9a} $$

Due to the kinematics, for a given end-effector initial position, $\mathbf{q}_{\mathbf{in}}$ is a continuous function of $\boldsymbol{\varepsilon}_{\mathbf{in}}$, n_{in}. Then (9a) takes the form

$$ S = S\left(t; \boldsymbol{\varepsilon}_{\mathbf{in}}, n_{\mathrm{in}}\right). \tag{9b} $$

Similarly, the time derivative of S has the form

$$ \dot{S} = f\left(t; \boldsymbol{\varepsilon}_{\mathbf{in}}, n_{\mathrm{in}}\right). \tag{10} $$

The function S can have a minimum either at a path intermediate point (Case I)—i.e., at some $t^* < t_{\mathrm{f}}$, where t_f is the final motion time—or at a path extreme point (Case II)—i.e., at either $t^* = 0$ (if this point is the initial one) or $t^* = t_{\mathrm{f}}$ (if this point is the final one).

In Case I, t^* can be found by setting $\dot{S}$ equal to 0:

$$ t^* = g\left(\boldsymbol{\varepsilon}_{\mathbf{in}}, n_{\mathrm{in}}\right). \tag{11} $$

For the desired path, the corresponding minimum of S is

$$ S_{\min} = S\left(t^*, \boldsymbol{\varepsilon}_{\mathbf{in}}, n_{\mathrm{in}}\right) = S\left(\boldsymbol{\varepsilon}_{\mathbf{in}}, n_{\mathrm{in}}\right). \tag{12a} $$

In Case II and for the desired path, the minimum of S is

$$ S_{\min} = S\left(t^*, \boldsymbol{\varepsilon}_{\mathbf{in}}, n_{\mathrm{in}}\right), \tag{12b} $$

where $t^* = 0$ or $t^* = t_{\mathrm{f}}$. Therefore, in all cases, for a desired path of given duration, the minimum of S is a continuous function of the initial spacecraft attitude:

$$ S_{\min} = S\left(\boldsymbol{\varepsilon}_{\mathbf{in}}, n_{\mathrm{in}}\right). \tag{13a} $$

For planar systems, (13a) is simplified to

$$ S_{\min} = S\left(\theta_{0,\mathrm{in}}\right), \tag{13b} $$

where $\theta_{0,\mathrm{in}}$ is the initial spacecraft attitude.

Next, the conditions that guarantee singularity avoidance are derived and illustrated geometrically.

In Case I the manipulator configuration $\mathbf{q}$, which corresponds to a minimum value of $S(\mathbf{q})$, is computed by setting the time derivative of $S(\mathbf{q})$ equal to 0:

$$ \dot{S} = \nabla S^{\mathrm{T}}\dot{\mathbf{q}} = 0, \tag{14} $$

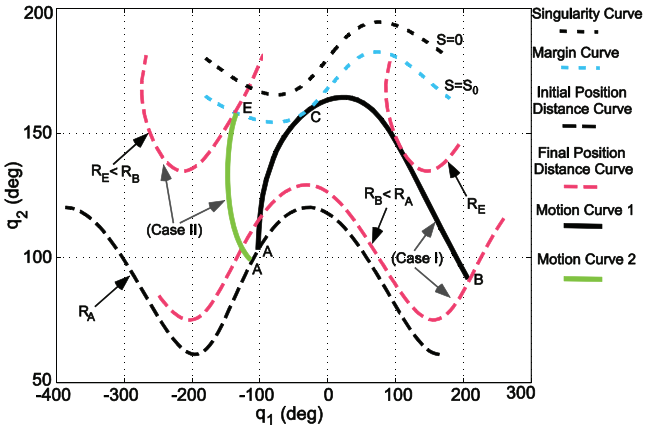

Fig. 3. Geometrical representation of minimum value of function S during end-effector motion along desired paths (Cases I, II). Case I: Minimum value S_0 corresponds to point C at which motion curve 1 is tangent to margin curve. Case II: Minimum value S_0 corresponds to final point E of motion curve 2 just touching margin curve.

where ∇S is the gradient of the scalar function $S(\mathbf{q})$. If the desired minimum value of S during the motion is S_0, then (14) and

$$S(\mathbf{q}) = S_0 \tag{15}$$

represent the necessary conditions for the computation of the manipulator configuration $\mathbf{q}$ such that $S_{\min} = S_0$.

In Case II, the minimum value of S corresponds to the initial or final value of S, or (respectively) equivalently to the end-effector initial or final position. Since the end effector's distance R from the origin (system center of mass) is a function of the manipulator configuration only [3], the equation

$$R(\mathbf{q}) = R_i, \tag{16}$$

where R_i is the radius of the initial or final end-effector position, along with (15) constitutes the necessary conditions for the computation of the manipulator configuration $\mathbf{q}$ such that $S_{\min} = S_0$.

Fig. 3 illustrates geometrically the conditions corresponding to Cases I and II. This figure shows the singularity ($S_0 = 0$) and margin ($S_0 \neq 0$) curves defined in Section II for the system in Fig. 2b. It also shows two additional joint space curves. The first is called the motion curve and depicts the manipulator configuration trace according to (8), during end-effector motion along a desired path (see motion curves 1 and 2 in Fig. 3; these curves correspond to end-effector motion along the paths AB and AE in Fig. 2b, respectively). The second curve, called the distance curve (for planar systems) or distance surface (for spatial systems), depicts manipulator configurations corresponding to a given end-effector distance from the system center of mass. For example, curves R_A, R_B, and R_E correspond to points A, B, and E in Fig. 2b, respectively.

Since the normal vector of a margin surface (or curve, for planar systems) is equal to the gradient ∇S of the scalar function $S(\mathbf{q})$ and the tangent vector of the motion curve is $\dot{\mathbf{q}}$, then in Case I, (14) indicates that the vectors $\dot{\mathbf{q}}$ and ∇S are normal to each other—or else that the motion curve and a margin surface (or curve) have a common tangent, as is the case with motion curve 1 in Fig. 3. In Case II, the minimum value of S corresponds to its initial or final value—or else the initial or final point of the motion curve should just touch the margin curve, as is the case with motion curve 2 in Fig. 3. Note that a DS only appears if the motion curve intersects the singularity surface (or curve). Note that different singularity surfaces (or curves) correspond to PDW A and B (see curves I and II in Fig. 2a). Therefore, if the end-effector path crosses both PDW areas, the motion curve should avoid intersection with both surfaces (curves) that correspond to these areas.

V. METHODOLOGY DEVELOPMENT FOR PLANAR SYSTEMS

Based on the previous analysis, in this section we develop a DS avoidance methodology for planar systems which yields appropriate initial spacecraft attitude ranges and is applicable to any desired end-effector path crossing both the PDW A and B areas.

To avoid DSs with some margin S_0, the initial spacecraft attitude values $\theta_{0,\text{in}}$, which correspond to $S_{\min} = S_0 > 0$, are computed first. In Section V.A, the computation of the values $\theta_{0,\text{in}}$ is presented analytically for a planar 3-dof manipulator with nonzero angular momentum. Using these values as limits, in Section V.B we define the initial spacecraft attitude ranges for DS avoidance in a single PDW area (A or B in Fig. 2b). Since the desired end-effector paths may cross both PDW areas A and B, in Section V.C the computation of the initial spacecraft attitude ranges is expanded to paths lying in both the PDW A and B areas.

A. Computation of the Range Limits

In this section a methodology to compute the limits $\theta_{0,\text{in}}$ is developed. This computation is based on the conditions described in Section IV (Cases I and II). The method is applied to planar systems with nonzero angular momentum, with the end-effector following any desired path with a desired orientation. To be able to specify both end-effector position and orientation, a 3-dof ($N = 3$) manipulator is used (see Fig. 4).

Using any kinetics method, such as the barycentric vector approach [3], the end-effector position and orientation for a 3-dof planar manipulator can be written as

$$x_E = ac_{(\theta_0)} + bc_{(\theta_0+q_1)} + cc_{(\theta_0+q_1+q_2)} + dc_{(\theta_0+q_1+q_2+q_3)} = x_E(s) \tag{17a}$$

$$y_E = as_{(\theta_0)} + bs_{(\theta_0+q_1)} + cs_{(\theta_0+q_1+q_2)} + ds_{(\theta_0+q_1+q_2+q_3)} = y_E(s) \tag{17b}$$

$$\theta_E = \theta_0 + q_1 + q_2 + q_3 = \theta_E(s), \tag{17c}$$

where a, b, c, and d are barycentric vector lengths, which reflect both the geometric configuration and the system

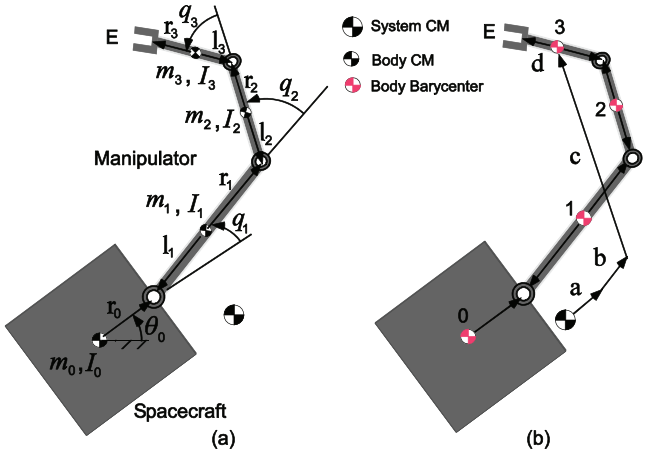

Fig. 4. (a) Definition of system mass properties and configuration parameters. (b) System barycentric vectors **a**, **b**, **c**, and **d** [3].

mass distribution (see Fig. 4b). The computation of the barycentric vectors is given in [3]. Also, $c_{(\cdot)} = \cos(\cdot)$, $s_{(\cdot)} = \sin(\cdot)$, and s is the arclength parameterization of the path ($0 \le s \le 1$), given by

$$s = \mathrm{a}_0 + \mathrm{a}_1 \mathrm{t} + \mathrm{a}_2 \mathrm{t}^2 + \mathrm{a}_3 \mathrm{t}^3 + \mathrm{a}_4 \mathrm{t}^4 + \mathrm{a}_5 \mathrm{t}^5. \tag{18a}$$

The initial and final values are $s_{\mathrm{in}} = 0$ and $s_{\mathrm{fin}} = 1$, respectively, and the initial and final velocities and accelerations are all zero.

Under these conditions, s is given by

$$s = 10\tau^3 - 15\tau^4 + 6\tau^5, \tag{18b}$$

where τ is the dimensionless time,

$$\tau = t t_{\mathrm{f}}^{-1}, \quad 0 \le \tau \le 1. \tag{19}$$

Since the orientation of the end-effector is specified, (17) can be written as

$$x_3 = x_E - d c_{(\theta_E)} = a c_{(\theta_0)} + b c_{(\theta_0+q_1)} + c c_{(\theta_0+q_1+q_2)} \tag{20a}$$

$$y_3 = y_E - d s_{(\theta_E)} = a s_{(\theta_0)} + b s_{(\theta_0+q_1)} + c s_{(\theta_0+q_1+q_2)}, \tag{20b}$$

where x_3, y_3 are the coordinates of point 3 (barycenter of link 3) in Fig. 4b.

For this system, the determinant of the generalized Jacobian given by (7) is

$$\begin{aligned} \det\left(\mathbf{S}^*\right) &= S(q_1, q_2) = abD_2 s_{(q_1)} + bcD_0 s_{(q_2)} \\ &\quad - acD_1 s_{(q_1+q_2)}, \\ &= k_0(q_1) + k_1(q_1)\, s_{(q_2)} + k_2(q_1)\, c_{(q_2)} \end{aligned} \tag{21a}$$

where $k_0(q_1)$, $k_1(q_1)$, and $k_2(q_1)$ are given in Appendix B.

Note that (21a) does not depend on q_3 and is identical with the singularity equation of a 2-dof manipulator [32], if one considers point 3 (Fig. 4b) as an end-effector. The influence of third-link mass is contained in the coefficients k_i ,$i = 0, 1, 2$. Therefore, the singularity-avoidance problem of a 3-dof manipulator with desired end-effector orientation is reduced to a 2-dof problem, if one considers the motion of manipulator point 3. The motion of point 3 is defined by the desired end-effector path and its orientation—see (20).

It can be shown that the equation

$$S(q_1, q_2) = \mathrm{S}_0 \tag{21b}$$

has the following solutions:

$$\begin{aligned} q_2(q_1) = \pi &- \arcsin\left[(\mathrm{S}_0 - \mathrm{k}_0)\Big/\sqrt{\mathrm{k}_1^2 + \mathrm{k}_2^2}\right] \\ &- \arctan\left(k_2/k_1\right), \end{aligned} \tag{22a}$$

corresponding to the singularity curve I ($\mathrm{S}_0 = 0$) or to the margin curve III ($\mathrm{S}_0 > 0$)—see Fig. 2a—and

$$q_2(q_1) = \arcsin\left[(\mathrm{S}_0 - \mathrm{k}_0)\Big/\sqrt{\mathrm{k}_1^2 + \mathrm{k}_2^2}\right] - \arctan\left(\mathrm{k}_2/\mathrm{k}_1\right), \tag{22b}$$

corresponding to the singularity curve II ($\mathrm{S}_0 = 0$) or to the margin curve IV ($\mathrm{S}_0 > 0$)—see Fig. 2a. Equation (22a) corresponds to a manipulator DS occurring in the PDW A are shown in Fig. 2b, and (22b) corresponds to a DS in the PDW B area. In Fig. 2a, the margin curves corresponding to $\mathrm{S}_0 < 0$ are drawn.

Next we derive analytically the conditions necessary to find the system configuration that corresponds to a minimum of the function S (Case I or II). The margin curve is defined by the value of S_0. The slope of the margin curve is found using the time derivative of (21b) and is given by

$$\lambda_1 = -\frac{\partial S(q_1, q_2)}{\partial q_1}\left(\frac{\partial S(q_1, q_2)}{\partial q_2}\right)^{-1} = g_1(q_1, q_2). \tag{23a}$$

The slope of the motion curve at some point (q_1, q_2) is

$$\lambda_2 = dq_2/dq_1 = \dot{q}_2/\dot{q}_1. \tag{23b}$$

The joint rates are expressed as a function of the spacecraft attitude, manipulator configuration, and end-effector path. Applying (8) on a 3-dof planar manipulator yields

$$\left[\dot{\theta}_0\ \dot{q}_1\ \dot{q}_2\ \dot{q}_3\right]^{\mathrm{T}} = \left[\dot{\theta}_0\ \dot{\mathbf{q}}^{\mathrm{T}}\right]^{\mathrm{T}} = \mathbf{T}(\theta_0, \mathbf{q})\left[h_{CM}\ \dot{x}_E\ \dot{y}_E\ \dot{\theta}_E\right]^{\mathrm{T}}, \tag{24}$$

where the 4×4 matrix $\mathbf{T}(\theta_0, \mathbf{q})$ is a function of the system configuration. The end-effector linear and angular velocities can be found by differentiating (17):

$$\left[\dot{x}_E\ \dot{y}_E\ \dot{\theta}_E\right]^{\mathrm{T}} = \left[\frac{\partial x_E}{\partial s}\ \frac{\partial y_E}{\partial s}\ \frac{\partial \theta_E}{\partial s}\right]^{\mathrm{T}} \dot{s}(t) = \mathbf{F}(s)\,\dot{s}(t). \tag{25}$$

Taking the second and the third equation of (24)—corresponding to $\dot{q}_1$ and $\dot{q}_2$, respectively—and using (25), (18b), and (19), we can write (23b) as

$$\lambda_2 = g_2(\theta_0, \mathbf{q}, \tau, h_{CM}, t_{\mathrm{f}}). \tag{26}$$

To avoid singularities in the PDW A or B areas, the motion curve and the margin curves—given by (22a) and (22b), respectively—must have a common tangent (see motion curve 1 in Fig. 3). If the subscript t denotes the system quantities at the touch point, then

$$\lambda_1(q_{1t}, q_{2t}) = \lambda_2(\theta_{0t}, \mathbf{q}_t, \tau_t, h_{CM}, t_{\mathrm{f}}). \tag{27}$$

Note that unlike the case of zero angular momentum [32], in the presence of nonzero angular momentum the singularity-avoidance problem depends on the motion's final time t_f, as shown by (27).

For a known value of angular momentum h_{CM} and a predefined final time t_f, the path equation in conjunction with (20), (17c), (18b), (22a) or (22b), and (27) comprise a nonlinear system in terms of $\theta_0, q_1, q_2, q_3, \tau$. Since (27) yields system configurations that correspond to both minimum and maximum values of S, in order to accept only those which correspond to $S = S_{\min}$ one should use the derived system configuration $(\theta_{0,t}, \mathbf{q_t})$ as initial conditions and solve (24) backwards (with motion time $\tau_t t_f$) and forwards (with motion time $(1 - \tau_t)t_f$) to the initial and final point, respectively, of the path given by (18a) and (25). Note that the backwards solution of (24) demands that the system angular momentum be used with the opposite sign. If in both directions the resulting motion curve does not intersect the singularity curve, then these solutions are accepted. In this case, the backwards solution yields the desired initial system configuration that bounds the range of feasible configurations.

In the case where (20), (17c), (18b), (22a) or (22b), and (27) in conjunction with the path equation yield no solution, there is no common tangent. Therefore, to avoid contact with the singularity curve, the final point of the motion curve must touch a margin curve given by (22a) or (22b), depending on the PDW area (see motion curve 2 in Fig. 3). In this case, the touch point (q_{1t}, q_{2t}) is the intersection point between the margin curve, given by (22a) or (22b), and the distance curve of the manipulator point 3, which using (20) is given by

$$R = \sqrt{a^2 + b^2 + c^2 + 2abc_{(q_1)} + 2acc_{(q_1+q_2)} + 2bcc_{(q_2)}}. \tag{28}$$

Equations (22a) or (22b), with (16) and (28), give the joint angles (q_{1t}, q_{2t}). The remaining variables (θ_{0t}, q_{3t}) can be found using (17), considering the end-effector final position and orientation. Using the derived solutions as initial conditions and solving (24) backwards (with motion time t_f) to the initial point of the path given by (18a) and (25) yields the desired initial system configuration that bounds the range of feasible configurations.

B. Initial Attitude Ranges for a Single PDW Area

In this section, the feasible ranges of initial spacecraft attitudes leading to DS avoidance during end-effector motion along paths lying in a single PDW area are established. As shown in Appendix C, the number of values of $\theta_{0,\text{in}} \in [0, 2\pi)$ corresponding to $S_{\min} = S_0$ is even. Consider that there are n values $\theta^i_{0,\text{in}} \in [0, 2\pi), i = 1, \ldots, n$, with $\theta^i_{0,\text{in}} < \theta^{i+1}_{0,\text{in}}$, which correspond to $S_{\min} = S_0 > 0$. Due to the continuity of the function S with respect to $\theta_{0,\text{in}}$, there are attitudes in the vicinity of $\theta^i_{0,\text{in}}$ which result in $S_{\min} > S_0$ and others which result in $S_{\min} < S_0$. These attitude values define ranges with boundary values $\theta^i_{0,\text{in}}$. Of those, the ranges which lead to DS avoidance are those for which $S_{\min} > S_0$.

Next, and without loss of generality, consider $n = 2$—i.e., that there are two values $\theta^1_{0,\text{in}}, \theta^2_{0,\text{in}} \in [0, 2\pi)$ corresponding to $S_{\min} = S_0$. To identify the feasible ranges, one can choose an arbitrary value $\theta^{*1}_{0,\text{in}} \in (\theta^1_{0,\text{in}}, \theta^2_{0,\text{in}})$. If the value $\theta^{*1}_{0,\text{in}}$ results in $S_{\min} > S_0$, then all attitudes in the chosen range $(\theta^1_{0,\text{in}}, \theta^2_{0,\text{in}})$ result in $S_{\min} > S_0$. Then the attitudes inside the adjacent ranges correspond to $S_{\min} < S_0$. Therefore, the desired range in $[0, 2\pi)$ which results in DS avoidance is defined by $\Theta = [\theta^1_{0,\text{in}}, \theta^2_{0,\text{in}}]$. Otherwise, the desired range is the complementary one, defined by $\Theta = [0, \theta^1_{0,\text{in}}] \cup [\theta^2_{0,\text{in}}, 2\pi)$.

In the general case, where n values $\theta^i_{0,\text{in}}$ correspond to $S_{\min} = S_0$, these ranges are given, respectively, by

$$\Theta = \bigcup_{k=0}^{k=(n-2)/2} \left[\theta^{2k+1}_{0,\text{in}}, \theta^{2k+2}_{0,\text{in}}\right] \tag{29a}$$

and

$$\Theta = \bigcup_{k=0}^{k=n/2} \left[\theta^{2k}_{0,\text{in}}, \theta^{2k+1}_{0,\text{in}}\right], \tag{29b}$$

where $\theta^0_{0,\text{in}} = 0$ rad and $\theta^{n+1}_{0,\text{in}} = 2\pi$ rad.

C. Initial Attitude Ranges for Multiple PDW Areas

We now tackle the problem of end-effector motion along any desired path, which may contain segments in both the PDW A and B areas and for a number of times. The path is divided into L successive parts, with their common points selected to lie in the PIW area. The number L is defined as equal to the number of times the end-effector path crosses the PDW. For example, the path segments AB and AF in Fig. 2b cross the PDW areas one and two times, respectively. Therefore, the path AF is divided into two segments AB and BF. The individual common points of the path segments are labeled by $0, 1, \ldots, L$, starting from the final point of the path (see Fig. 2b). The common points for segment i are points $i - 1$ and i. This procedure results in distinct path segments crossing a single PDW area. The feasible attitude ranges leading to DS avoidance in a single area were defined in Section V.B. Next, the range notation is generalized, with the end-effector starting at point k and avoiding DSs along path segment l, as Θ^k_l.

For example, in Fig. 2b the end-effector is driven from point 2 to point 0. To find the feasible spacecraft attitudes at point 2 that avoid any DS, the path AF is divided into segments BF (path segment 1) and AB (path segment 2). Both segments cross a single PDW area. The feasible spacecraft attitude range Θ^1_1 at point 1 that avoids DSs at path segment 1 is computed first. Then the feasible spacecraft attitude range Θ^1_2 at the same point is computed so as to avoid DSs at path segment 2**.** The intersection $\Theta^1_{1\&2} = \Theta^1_1 \cap \Theta^1_2$ yields the feasible spacecraft attitude range at point 1 that avoids DSs at both path segments

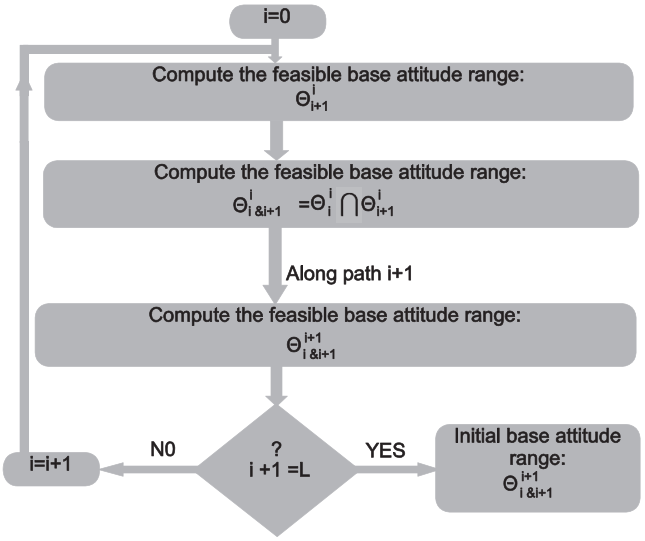

Fig. 5. Flowchart for end-effector path that crosses both PDW A and B areas.

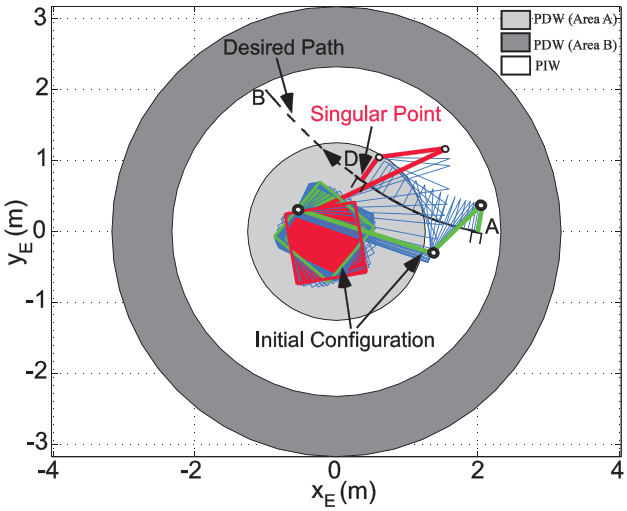

Fig. 6. Motion animation of space manipulator motion with $\theta_0^{\text{in}} = 140^\circ$.

TABLE I
Parameters of the System Shown in Fig. 4

Body	l_i (m)	r_i (m)	m_i (kg)	I (kg·m^2)
0	0.5	0.5	400	66.67
1	1.0	1.0	40	3.33
2	0.5	0.5	30	2.50
3	0.2	0.2	1	1.5

1 and 2. Then the reverse motion from point 1 to point 2 along path segment 2 yields the feasible attitude range $\Theta^2_{1\&2}$ at point 2. Since the range $\Theta^1_{1\&2}$ results in DS avoidance in both segments 1 and 2, the range $\Theta^2_{1\&2}$ guarantees DS avoidance along path AF (point 2 to point 0).

Fig. 5 illustrates the methodology concept as a flowchart. Since no path segment 0 exists, we set $\Theta^0_0 = [0, 2\pi]$ and $\Theta^1_{0\&1} = \Theta^1_1$. The output is the range of initial attitudes which guarantee DS avoidance during end-effector motion.

Therefore, the proposed method yields the feasible initial spacecraft attitude ranges for planar systems, so that DSs during given end-effector motion are avoided. The developed method is illustrated by an example.

Example 1 To illustrate the developed method, the planar space manipulator system in Fig. 4 with parameters in Table I is employed. The third link corresponds to a small orientation link whose position and orientation should follow the desired trajectory. This link is then a small-mass rigid body. A larger link with a higher mass can be used, since the feasibility of the proposed method is not affected by specific system inertial properties. The initial angular momentum of the robot is $h_0 = 0.5$ N·m·s. It is desired that the end-effector moves from point $A = (2.0, 0.0)$ m to point $B = (-1.0, 2.0)$ m following a parabolic path and intermediate point $C = (0.0, 1.0)$ m in time $t_f = 100$ s. The path is given by

$$y_E = \alpha x_E^2 + \beta x_E + \gamma, \tag{30a}$$

where one can set

$$x_E(\theta_0(t), \mathbf{q}(t)) = x_{\text{in}} + (x_{\text{fin}} - x_{\text{in}})\, s(t) \tag{30b}$$

with x_{in} and x_{fin} corresponding to end-effector initial and final positions, respectively. In addition, the third link is required to be normal to the path.

Next, the appropriate initial configurations that guarantee DS avoidance are computed using the developed method. For the entire range of q_1 and q_2, the maximum value of S is $S_{\max} \approx 150$. We choose $S_0 = 5$ ($S_0 \approx 3.3\%$ of $S_{\max}$) to obtain a satisfactory range of spacecraft feasible attitudes. Note that one can also select a negative value of S_0.

To satisfy the normality condition, the end-effector attitude should be given by

$$\theta_E = 3\pi/2 + \arctan\left(\partial y_E(x_E)/\partial x_E\right). \tag{30c}$$

Since only the motion of point 3 may cause a DS, the PIW and PDW areas in Figs. 6 and 7 have been computed based on its motion. Point 3 crosses both the PDW A and B areas once (see Fig. 7). Then $L = 2$. First, the end-effector path AB is divided into path segments AF and FB, where $F = (-0.5, 1.4583)$ m and the corresponding position F' of point 3 belongs to the PIW area (see Fig. 7). Since the system's angular momentum is nonzero, the motion duration must be taken into account. In this case, (18b), (19), and (30b) result in the time duration $t_1 = 69.73$ s and $t_2 = t_f - t_1$, respectively, for the path segments AF and FB.

Applying the procedure described by the flowchart in Fig. 5, first the feasible attitude range at final point B is computed in order to avoid a DS at path FB. According to Section V.A, the acceptable spacecraft attitude, manipulator configuration, and dimensionless time at

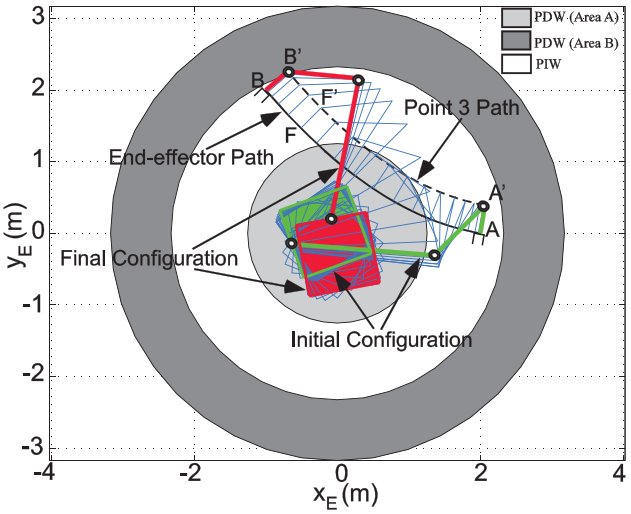

Fig. 7. Motion animation of space manipulator motion with $\theta_0^{\text{in}} = 200°$.

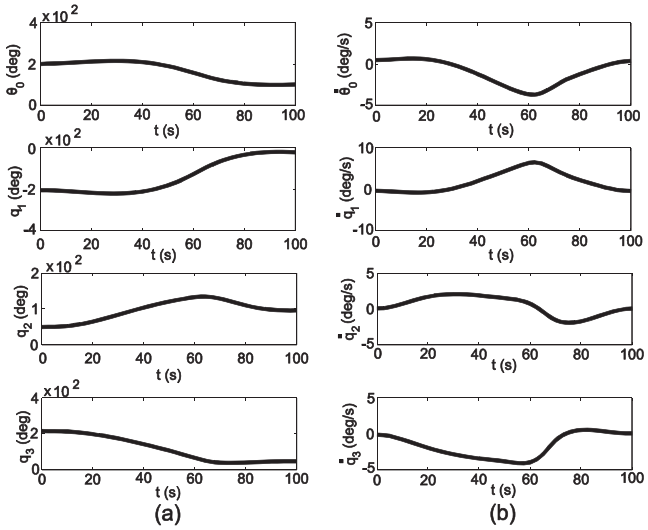

Fig. 8. For motion in Fig. 7, (a) spacecraft attitude and joint angle trajectories and (b) spacecraft attitude and joint angle rates.

which the motion curve is tangent to the margin curve $S = \mathrm{S}_0$ are computed as

$$\left[\theta_{0,t}, \mathbf{q}_t^{\mathrm{T}}\right]^{\mathrm{T}} = [-0.7463, -3.6512, 0.1762, 1.7885]^{\mathrm{T}} \text{ rad},$$
$$\tau_t = 0.9495.$$

In this case, the spacecraft attitude at point B is $\theta_0^B = 318.9°$.

Since the motion curve does not have another common tangent with the margin curve at the PDW B area, the motion curve should touch the margin curve when the end-effector arrives at point B. Application of the procedure described in Section V.A yields the acceptable solution of $\theta_0^B = 259.4°$.

The aforementioned spacecraft attitudes θ_0^B bound the spacecraft attitude range at point B, and according to Section V.B, the feasible attitude range at point B is $\Theta_{FB}^B = [0°, 259.4°] \cup [318.9°, 360°]$. The reverse motion from point B to F of path segment FB then yields the feasible range at point F: $\Theta_{FB}^F = [0°, 298.7°] \cup [354.2°, 360°]$.

Next, the feasible spacecraft attitude range at F is computed to avoid a DS at path AF. The acceptable spacecraft attitude, manipulator configuration, and dimensionless time at which the motion curve is tangent to the margin curve $S = \mathrm{S}_0$ are

$$\left[\theta_{0t}, \mathbf{q}_t^{\mathrm{T}}\right]^{\mathrm{T}} = [0.9158, -0.6074, 2.9265, 0.9617]^{\mathrm{T}} \text{ rad},$$
$$\tau_t = 0.4895$$

$$\left[\theta_{0t}, \mathbf{q}_t^{\mathrm{T}}\right]^{\mathrm{T}} = [1.5922, -0.7348, 2.9014, 0.2833]^{\mathrm{T}} \text{ rad},$$
$$\tau_t = 0.6413.$$

Therefore, the initial spacecraft attitudes at point F are $\theta_0^F = 335.3°$ and $\theta_0^F = 60.9°$, respectively, and the feasible spacecraft attitude range at point F that avoids a DS at path segment AF is $\Theta_{AF}^F = [60.9°, 335.3°]$.

The spacecraft attitude range at point F that guarantees DS avoidance at both the path segments AF and FB is $\Theta_{AF\&FB}^F = \Theta_{AF}^F \cap \Theta_{FB}^F = [60.9°, 298.7°]$. The reverse motion from point F to point A of segment AF then results in spacecraft attitude limits $\theta_0^A = 161°$ and $\theta_0^A = 63°$. The spacecraft attitude range at point A that avoids a DS along path AB is given by $\Theta_{AB}^A = [0°, 63°] \cup [161°, 360°]$. This range can be increased if a smaller value for S_0 is selected.

Figs. 6 and 7 show the system motion when the initial spacecraft orientation is $\theta_0^{\text{in}} = 140°$ and $\theta_0^{\text{in}} = 200°$, respectively. In the first case, the initial attitude is outside the boundaries we have computed, and therefore the desired motion is not feasible (the manipulator becomes singular at point D). In the second case, the initial base orientation permits the end-effector to follow the desired path. Figs. 8a, 8b show the resulting trajectories and their rates, respectively.

VI. METHODOLOGY DEVELOPMENT FOR SPATIAL SYSTEMS

In this section, the method described in Section IV is extended to spatial systems such as the free-floating space manipulator shown in Fig. 1. It is desired that the end-effector follow an arbitrary path connecting two points with appropriate orientation. The specification of a desired end-effector orientation requires a 6-dof spatial manipulator. The end-effector position and orientation are given by

$$\mathbf{r_E} = \left[\, x_E(\boldsymbol{\varepsilon}, n, \mathbf{q}) \quad y_E(\boldsymbol{\varepsilon}, n, \mathbf{q}) \quad z_E(\boldsymbol{\varepsilon}, n, \mathbf{q}) \,\right]^{\mathrm{T}}$$
$$= \left[\, x_E(s) \quad y_E(s) \quad z_E(s) \,\right]^{\mathrm{T}} \tag{31a}$$
$$\mathbf{R_E}(\boldsymbol{\varepsilon}, n, \mathbf{q}) = \mathbf{R_E}(s), \tag{31b}$$

where $\mathbf{R_E}$ is the rotation matrix that describes the orientation of the end-effector with respect to the inertial frame, the arclength parameterization s of the path is given by (18), and the unit quaternion $\boldsymbol{\varepsilon}, n$ satisfies the constraint

$$\boldsymbol{\varepsilon}^{\mathrm{T}}\boldsymbol{\varepsilon} + n^2 = 1. \tag{32}$$

TABLE II
Parameters of the System Shown in Fig. 1

Body	l_i (m)	r_i (m)	m_i (kg)	I_{xx} (kg·m^2)	I_{yy} (kg·m^2)	I_{zz} (kg·m^2)
0	–	$[0, 0, 0.5]^{\mathrm{T}}$	400	66.67	66.67	66.67
1	0	0	0	0	0	0
2	0.5	0.5	40	0.001	2.5	2.5
3	0.5	0.5	30	0.001	7.5	1.7
4	0	0	0	0	0	0
5	0	0	0	0	0	0
6	0.2	0.2	10	1.5	1.5	1.5

The end-effector velocity is simply

$$\dot{\mathbf{r}}_{\mathbf{E}} = \begin{bmatrix} \partial x_E/\partial s & \partial y_E/\partial s & \partial z_E/\partial s \end{bmatrix}^{\mathrm{T}} \dot{s} = \mathbf{F}\dot{s} \tag{33a}$$

$$\boldsymbol{\omega}_{\mathbf{E}}^{\times} = \dot{\mathbf{R}}_{\mathbf{E}}\mathbf{R}_{\mathbf{E}}^{\mathbf{T}}, \tag{33b}$$

where $\boldsymbol{\omega}_{\mathbf{E}}^{\times}$ is the skew symmetric matrix obtained from the end-effector angular velocity vector $\boldsymbol{\omega}_{\mathbf{E}}$.

The determinant of the generalized Jacobian in (7) is

$$S(\mathbf{q}) = \det\left(\mathbf{S}^*\right) = S(q_1, q_2, q_3, q_4, q_5, q_6) \tag{34}$$

and represents a surface in the 6-dimensional joint space.

For a known value of angular momentum h_{CM} and a predefined final time t_{f}, the path equation in conjunction with (31), (18b), (32), (34), and (14) can be solved to yield the variables $\boldsymbol{\varepsilon}, n, \mathbf{q}, \tau$.

The representation of the singularity surfaces in a 6-dimensional joint space is complex. However, the analysis is simplified using a 3-dof manipulator equipped with a spherical wrist. For this manipulator, the end-effector position is

$$\mathbf{r}_{\mathbf{E}} = \mathbf{r_3} + \mathbf{R_0}\,{}^{\mathbf{0}}\mathbf{R_6}\,{}^{\mathbf{6}}\mathbf{u}_{\mathbf{6,E}} = \mathbf{r_3} + \mathbf{R_E}\,{}^{\mathbf{6}}\mathbf{u}_{\mathbf{6,E}}, \tag{35}$$

where $\mathbf{r_3}$ is the position of the third-link barycenter (point 3 in Fig. 1), ${}^{\mathbf{0}}\mathbf{R_6}$ is the rotation matrix between the last-link frame and the spacecraft frame, and ${}^{\mathbf{6}}\mathbf{u}_{\mathbf{6,E}}$ is the fixed barycentric vector which corresponds from the third-link barycenter to the end-effector.

Since the orientation of the end-effector is specified, (35) can be written as

$$\mathbf{r_3}(\boldsymbol{\varepsilon}, n, q_1, q_2, q_3) = \mathbf{r_E} - \mathbf{R_E}\,{}^{\mathbf{6}}\mathbf{u}_{\mathbf{6,E}}. \tag{36}$$

Therefore, the motion of the end-effector along a desired path with specific orientation results in a particular path for the manipulator point 3. For this manipulator, the determinant of the generalized Jacobian given in (7) is

$$S = \det\left(\mathbf{S}^*\right) = S(q_1, q_2, q_3). \tag{37}$$

Since (37) does not depend on wrist angles, according to (36) the singularity-avoidance problem of this manipulator with desired end-effector orientation is specified by the motion of manipulator point 3, and (14) is simplified to

$$\dot{q}_1\partial S/\partial q_1 + \dot{q}_2\partial S/\partial q_2 + \dot{q}_3\partial S/\partial q_3 = 0. \tag{38}$$

An analytic form of the singularities resulting from (37) can be derived for a manipulator mounted along a principal axis of the spacecraft and with the spacecraft moments of inertia about the two other principal axes equal. Then, the generalized Jacobian in (37) is

$$\mathbf{S}^*(q_1, q_2, q_3) = {}^{\mathbf{0}}\mathbf{R_1}(q_1)\,\mathbf{S_n}(q_2, q_3), \tag{39}$$

where ${}^{\mathbf{0}}\mathbf{R}_1$ is the rotation matrix between the first-link and spacecraft frames and $\mathbf{S_n}(q_2, q_3)$ is the new generalized Jacobian. Since ${}^{\mathbf{0}}\mathbf{R}_1$ is a rotation matrix, (37) and (39) yield

$$S = \det\left(\mathbf{S}^*\right) = \det\left(\mathbf{S_n}(q_2, q_3)\right) = S(q_2, q_3). \tag{40}$$

Therefore, the dynamic singularities do not depend on q_1. In addition, it can be shown that the equation $S(q_2, q_3) = \mathrm{S}_0$, where S_0 is a constant, has analytic solutions similar to the ones described by (22). For such systems, the singularity- and margin-surface shapes are independent of q_1 and have cross sections similar to the corresponding curves of planar systems shown in Fig. 2a. The PDW and PIW areas are spherical concentric volumes with cross sections similar to the workspace of planar systems shown in Fig. 2b.

In spatial systems, since the spacecraft attitude is described by three independent variables, the computation of the feasible ranges of these variables is not trivial. However, one can find individual attitude solutions that guarantee DS avoidance. This is next presented via an example.

Example 2 The spatial manipulator with a spherical wrist shown in Fig. 1 is employed, with parameters given in Table II. The 0s in Table II represent the massless body connecting the first two revolute joints and the spherical wrist. The end-effector moves from point $A = (1, 0, 0)$ m to point $B = (-0.50, 0.80, 0.33)$ m following a straight-line path in time $t_{\mathrm{f}} = 100$ s. The end-effector must be normal to the plane

$$0.4683x + 1.1683y - 0.7000z - 0.4683 = 0 \tag{41}$$

on which the straight-line path belongs. The initial angular momentum of the robot is $\mathbf{h_{CM}} = [\,0.5\ 0.3\ 0.1\,]^{\mathrm{T}}$ N·m·s. The path of manipulator point 3 in Fig. 1 crosses the PDW. An initial spacecraft attitude such as $\boldsymbol{\varepsilon}_{\mathbf{in}} = [\,0.1\ 0.5\ 0.2\,]^{\mathrm{T}}$, $n_{\mathrm{in}} = -0.8367$ (shown in Fig. 9a), results in an initial end-effector motion on the desired path (see Fig. 9b), to

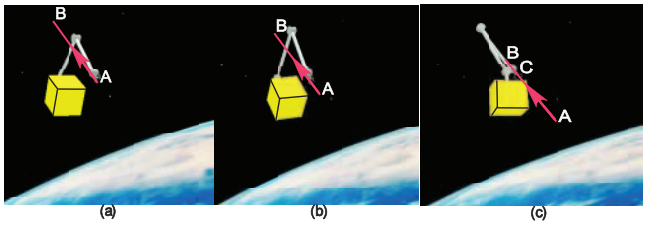

Fig. 9. System motion snapshots. System becomes singular at point C.

end at a manipulator dynamic singularity that occurs at point $C = (0.1214, 0.4686, 0.1943)$ m, as depicted in Fig. 9c.

Next, an appropriate initial configuration is computed that guarantees that no DS will be encountered. Since the path of point 3 crosses only one of the PDW areas, $L = 1$—i.e., there is one path segment only. For increased safety margins, $S_0 = -5$ is chosen. The corresponding manipulator configuration, spacecraft attitude, and dimensionless time at which the motion curve is tangent to the margin surface $S = S_0$ are found according to Section VI.

Setting $q_1 = 0.1$ rad, one acceptable solution is

$$\mathbf{q_t} = \begin{bmatrix} 0.1 & 2.0 & 3.3076 & -2.6104 & 2.2981 & 1.4288 \end{bmatrix}^{\mathrm{T}} \text{rad}$$

$$[\boldsymbol{\varepsilon_t}, n_t] = \begin{bmatrix} 0.4295 & -0.147 & 0.6898 & -0.564 \end{bmatrix}^{\mathrm{T}},$$
$$\tau_t = 0.4225.$$

An initial feasible spacecraft orientation is then

$$[\boldsymbol{\varepsilon_{in}}, n_{\mathrm{in}}] = \begin{bmatrix} 0.46 & 0.0935 & 0.7352 & -0.489 \end{bmatrix}^{\mathrm{T}}.$$

Using other values for q_1 results in additional solutions and eventually sets of such solutions. Since $S_0 < 0$ has been selected, these solutions correspond to $S_{\max} = S_0$. Similar to the planar case, the continuity of the function $S_{\max}$ results in ranges in the vicinity of $\boldsymbol{\varepsilon_{in}}, n_{\mathrm{in}}$ which correspond to $S_{\max} > S_0$ or $S_{\max} < S_0$. In this case, the ranges which lead to DS avoidance are those for which $S_{\max} < S_0$. However, as mentioned earlier, the computation of feasible full ranges is complex. This is an issue for future research.

This initial spacecraft orientation with the manipulator at point A results in end-effector motion on path AB without encountering DS, as shown in Fig. 10. The end-effector trajectories are shown in Fig. 11a, while Figs. 11b, 11c show the trajectories of the manipulator and wrist configuration variables, respectively. The spacecraft attitude expressed by x-y-z Euler angles is shown in Fig. 11d. Figs. 11e, 11f show the robot joint rates, and Fig. 11g shows the spacecraft angular velocity expressed in the inertial frame. It can be seen that all trajectories are smooth throughout the motion, and no dynamic singularities occur; the end-effector follows the path from the initial point A to the final point B.

Note that applying the proposed method requires solving a system of a few nonlinear algebraic equations

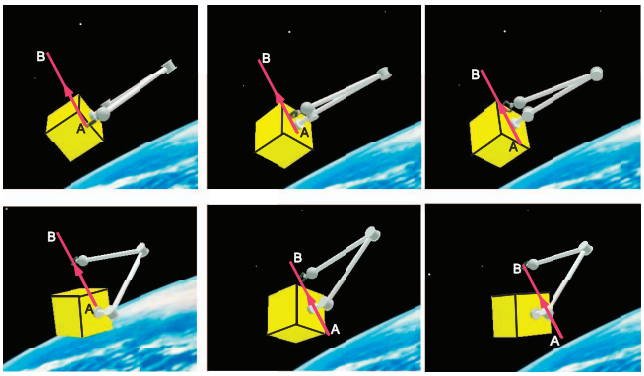

Fig. 10. System motion snapshots. End-effector follows path from A to B without encountering dynamic singularities.

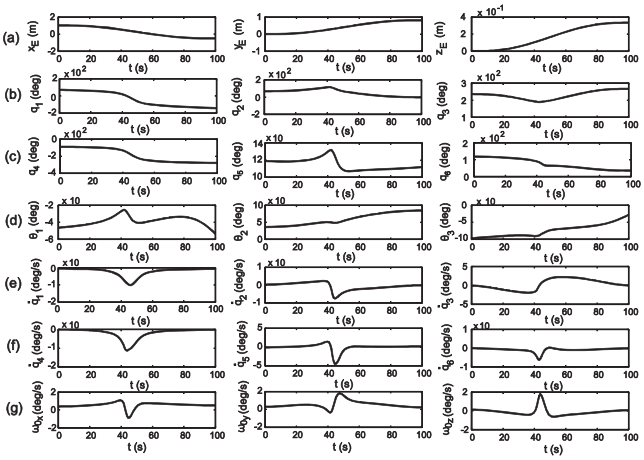

Fig. 11. (a) End-effector position trajectory. (b) Manipulator joint angle trajectories. (c) Wrist joint angle trajectories. (d) Spacecraft attitude trajectories (x-y-z Euler angles). (e) Manipulator joint angle rates. (f) Wrist joint angles rates. (g) Spacecraft angular velocity.

and knowledge of the system dynamics; it can be implemented with simple code running in MATLAB. Although parameters in space systems are known rather accurately, identification methods can be used to improve this knowledge. However, this is beyond the scope of this work.

VII. CONCLUSIONS

In this paper, a trajectory-planning method allowing the end-effector to follow a desired path avoiding DSs was developed. Since the path is predefined, the method yields the appropriate initial spacecraft attitude values that avoid dynamically singular configurations during the motion. Thus, the entire system workspace can be used. Here, a nonzero initial system angular momentum was assumed, and its influence on the end-effector trajectory planning was studied in order to guarantee the robustness of the method in the presence of angular momentum. Furthermore, the proposed method is applicable to any desired path and was applied to both planar and spatial systems allowing commands for both end-effector desired position and orientation. In addition to the computation of

feasible initial spacecraft attitudes, in planar systems the method also yielded the exact range of such attitudes. The application of the method was illustrated by two examples.

APPENDIX A

This appendix shows the property that the initial configuration is obtained if a trajectory is followed from its end to its beginning by reversing the end-effector motion and the sign of the angular momentum. Equations (8a), (8b), and (8c) yield

$$\dot{\mathbf{x}} = \mathbf{A_1}(\mathbf{x})\,\mathbf{h_{CM}} + \mathbf{A_2}(\mathbf{x})\,\dot{\mathbf{r}}_\mathbf{E}, \tag{42}$$

where $\dot{\mathbf{r}}_\mathbf{E}$ is given by (33a);

$$\mathbf{x} = \begin{bmatrix} \boldsymbol{\varepsilon}^{\mathrm{T}} & n & \mathbf{q}^{\mathrm{T}} \end{bmatrix}^{\mathrm{T}};$$

and

$$\mathbf{A_1}(\mathbf{x}) = \begin{bmatrix} \mathbf{E}\left[{}^{\mathbf{0}}\mathbf{D}^{-\mathbf{1}} + {}^{\mathbf{0}}\mathbf{D}^{-\mathbf{1}}\,{}^{\mathbf{0}}\mathbf{D}_\mathbf{q}\mathbf{S}^{-\mathbf{1}}\,{}^{\mathbf{0}}\mathbf{J}_{\mathbf{11}}\,{}^{\mathbf{0}}\mathbf{D}^{-\mathbf{1}}\right]\mathbf{R}_\mathbf{0}^{\mathrm{T}} \\ -\mathbf{S}^{-\mathbf{1}}\,{}^{\mathbf{0}}\mathbf{J}_{\mathbf{11}}\,{}^{\mathbf{0}}\mathbf{D}^{-\mathbf{1}}\mathbf{R}_\mathbf{0}^{\mathrm{T}} \end{bmatrix} \tag{43a}$$

$$\mathbf{A_2}(\mathbf{x}) = \begin{bmatrix} -\mathbf{E}\,{}^{\mathbf{0}}\mathbf{D}^{-\mathbf{1}}\,{}^{\mathbf{0}}\mathbf{D}_\mathbf{q}\mathbf{S}^{-\mathbf{1}}\mathbf{R}_\mathbf{0}^{\mathrm{T}} \\ \mathbf{S}^{-1}\mathbf{R}_\mathbf{0}^{\mathrm{T}} \end{bmatrix}, \tag{43b}$$

with

$$\mathbf{E} = \begin{bmatrix} (1/2)\left[\boldsymbol{\varepsilon}^{\times} + n\mathbf{I}\right] \\ -(1/2)\,\boldsymbol{\varepsilon}^{\mathrm{T}} \end{bmatrix}. \tag{43c}$$

Using (33a), (42) can be written as

$$d\mathbf{x} = \mathbf{A_1}(\mathbf{x}(\mathrm{t}))\,\mathbf{h_{CM}}\mathrm{dt} + \mathbf{A_2}\mathbf{x}(\mathrm{t})\,\mathbf{F}(\mathrm{s}(\mathrm{t}))\,\dot{\mathrm{s}}(\mathrm{t})\,\mathrm{dt}. \tag{44}$$

Suppose that the end-effector moves from A with base orientation and manipulator configuration described by $\mathbf{x}_1$ to B with base orientation and manipulator configuration described by $\mathbf{x}_2$, in $\Delta t = t_2 - t_1$. Integration of (44) yields

$$\int_{\mathbf{x}_1}^{\mathbf{x}_2} d\mathbf{x} = \mathbf{x}_2 - \mathbf{x}_1 = \int_{t_1}^{t_2} \mathbf{A_1}\mathbf{h_{CM}}\mathrm{dt} + \int_{t_1}^{t_2} \mathbf{A_2}\mathbf{F}\dot{s}\mathrm{dt}. \tag{45}$$

Then the end-effector starts from point B with base orientation and manipulator configuration described by $\mathbf{x}_2$ to point A with base orientation and manipulator configuration described by $\mathbf{x}_3$, at the same time $\Delta t = t_2 - t_1$ and with opposite angular momentum. The motion BA corresponds to opposite end-effector velocity. Integration of (44) yields

$$\int_{\mathbf{x}_2}^{\mathbf{x}_3} \mathrm{d}\mathbf{x} = \mathbf{x}_3 - \mathbf{x}_2 = -\int_{t_1}^{t_2} \mathbf{A_1}\mathbf{h_{CM}}\mathrm{dt} - \int_{t_1}^{t_2} \mathbf{A_2}\mathbf{F}\dot{s}\mathrm{dt}. \tag{46}$$

Comparison of (45) and (46) yields

$$\mathbf{x}_2 - \mathbf{x}_1 = -(\mathbf{x}_3 - \mathbf{x}_2) \Rightarrow \mathbf{x}_3 = \mathbf{x}_1. \tag{47}$$

APPENDIX B

The parameters $k_i, i = 0, 1, 2$, in (21a) are

$$k_0(q_1) = (2aba_{22} - c(aa_{21} + ba_{02}))\,s_{(q_1)}/2 \tag{48}$$

$$k_1(q_1) = -(aba_{02} + aca_{01} - 2bca_{00})/2 + c(-aa_{11} + ba_{01})\,c_{(q_1)} + a(ba_{02} - ca_{01})\,c_{(2q_1)}/2 \tag{49}$$

$$k_2(q_1) = a(ba_{21} - ca_{11})\,s_{(q_1)} + a(ba_{02} - ca_{01})\,s_{(2q_1)}/2, \tag{50}$$

where a, b, and c are the barycentric vector lengths. The term a_{ij} is equal to ${}^0d_{ij}$, but without the $c_{(\cdot)}$ terms. The scalars ${}^0d_{ij}$ result from the inertia matrices $\mathbf{{}^0D_{ij}}$ defined in [3].

APPENDIX C

We show that the number of values of $\theta_{0,\mathrm{in}} \in [0, 2\pi)$ that correspond to $S_{\min} = \mathrm{S}_0$ is even. Assume that there are n values of the initial spacecraft attitude $\theta^i_{0,\mathrm{in}} \in [0, 2\pi), i = 1, 2, \ldots, n$ and $\theta^i_{0,\mathrm{in}} < \theta^{i+1}_{0,\mathrm{in}}$, that correspond to $S_{\min} = \mathrm{S}_0 > 0$ and n arbitrary spacecraft attitudes $\theta^{*i}_{0,\mathrm{in}} \in [0, 2\pi)$ so that $\theta^{*i}_{0,\mathrm{in}} \in (\theta^i_{0,\mathrm{in}}, \theta^{i+1}_{0,\mathrm{in}})$, $i = 1, 2, \ldots, n$. Note that the values of $\theta^i_{0,\mathrm{in}}$ and $\theta^{*i}_{0,\mathrm{in}}$ are repeated after 2π so that the periodicity of the function S is satisfied. Then $\theta^{n+i}_{0,\mathrm{in}} = 2\pi + \theta^i_{0,\mathrm{in}}$ and $\theta^{*n+i}_{0,\mathrm{in}} = 2\pi + \theta^{*i}_{0,\mathrm{in}}$. Next, the function $f(\theta_{0,\mathrm{in}}) = S_{\min}(\theta_{0,\mathrm{in}}) - \mathrm{S}_0$ is defined. Since this function is continuous with respect to $\theta_{0,\mathrm{in}}$ and has solutions $\theta^i_{0,\mathrm{in}}$, the following n inequalities hold:

$$\begin{aligned} f\left(\theta^{*1}_{0,\mathrm{in}}\right) f\left(\theta^{*2}_{0,\mathrm{in}}\right) < 0 &\Rightarrow -\frac{f\left(\theta^{*1}_{0,\mathrm{in}}\right)}{f\left(\theta^{*2}_{0,\mathrm{in}}\right)} > 0 \\ &\vdots \\ f\left(\theta^{*n}_{0,\mathrm{in}}\right) f\left(\theta^{*n+1}_{0,\mathrm{in}}\right) < 0 &\Rightarrow -\frac{f\left(\theta^{*n}_{0,\mathrm{in}}\right)}{f\left(\theta^{*n+1}_{0,\mathrm{in}}\right)} > 0 \end{aligned} \tag{51}$$

Multiplying the n inequalities in (48) yields

$$\pm\frac{f\left(\theta^{*1}_{0,\mathrm{in}}\right)}{f\left(\theta^{*n+1}_{0,\mathrm{in}}\right)} > 0, \tag{52}$$

where the plus and minus signs correspond to even and odd values of n, respectively. Furthermore, $f(\theta_{0,\mathrm{in}})$ is periodic, so

$$f\left(\theta^{*n+1}_{0,\mathrm{in}}\right) = f\left(2\pi + \theta^{*1}_{0,\mathrm{in}}\right) = f\left(\theta^{*1}_{0,\mathrm{in}}\right). \tag{53}$$

Equations (49) and (50) yield

$$\pm 1 > 0. \tag{54}$$

However, (54) is true only for the case where the sign is positive. Therefore, the number n of the values of the initial spacecraft attitude that satisfy $S_{\min} = \mathrm{S}_0 > 0$ must be even.

REFERENCES

[1] Yoshida, K., Hashizume, K., and Abiko, S.
Zero reaction maneuver: Flight validation with ETS-VII space robot and extension to kinematically redundant arm.
In *IEEE International Conference on Robotics and Automation*, Seoul, Korea, May 2001, **1**, 441–446.

[2] Ogilvie, A., Allport, J., Hannah, M., and Lymer, J.
Autonomous satellite servicing using the Orbital Express Demonstration Manipulator System.
In *Proceedings of the 9th International Symposium on Artificial Intelligence, Robotics and Automation in Space*, Hollywood, CA, Feb. 2008.

[3] Papadopoulos, E., and Dubowsky, S.
Dynamic singularities in free-floating space manipulators.
Journal of Dynamic Systems, Measurement, and Control, **115**, 1 (Mar. 1993), 44–52.

[4] Xu, W., Liang, B., and Xu, Y.
Survey of modeling, planning, and ground verification of space robotic systems.
Acta Astronautica, **68**, 11–12 (2011), 1629–1649.

[5] Papadopoulos, E. G.
Path planning for space manipulators exhibiting nonholonomic behavior.
In *Proceedings of the 1992 IEEE/RSJ International Conference on Intelligent Robots and Systems*, Raleigh, NC, July 1992, **1**, 669–675.

[6] Vafa, Z., and Dubowsky, S.
On the dynamics of space manipulators using the Virtual Manipulator, with applications to path planning.
The Journal of the Astronautical Sciences, **38**, 4 (1990), 441–472.

[7] Papadopoulos, E., and Dubowsky, S.
On the nature of control algorithms for free-floating space manipulators.
IEEE Transactions on Robotics and Automation, **7**, 6 (Dec. 1991), 750–758.

[8] Umetani, Y., and Yoshida, K.
Workspace and manipulability analysis of space manipulator.
Transactions of the Society of Instrument and Control Engineers, **E-1**, 1 (2001), 116–123.

[9] Umetani, Y., and Yoshida, K.
Resolved motion rate control of space manipulators with generalized Jacobian matrix.
IEEE Transactions on Robotics and Automation, **5**, 3 (June 1989), 303–314.

[10] Caccavale, F., and Siciliano, B.
Kinematic control of redundant free-floating robotic systems.
Advanced Robotics, **15**, 4 (2001), 429–448.

[11] Franch, J., Agrawal, S. K., Oh, S., and Fattah, A.
Design of differentially flat planar space robots: A step forward in their planning and control.
In *2003 IEEE/RSJ International Conference on Intelligent Robots and Systems*, Las Vegas, NV, Oct. 2003, **3**, 3053–3058.

[12] Agrawal, S. K., Pathak, K., Franch, J., Lampariello, R., and Hirzinger, G.
A differentially flat open-chain space robot with arbitrarily oriented joint axes and two momentum wheels at the base.
IEEE Transactions on Automatic Control, **54**, 9 (Sept. 2009), 2185–2191.

[13] Tortopidis, I., and Papadopoulos, E.
On point-to-point motion planning for underactuated space manipulator systems.
Robotics and Autonomous Systems, **55**, 2 (Feb. 2007), 122–131.

[14] Pandey, S., and Agrawal, S. K.
Path planning of free-floating prismatic-jointed manipulators.
Multibody System Dynamics, **1**, 1 (Mar. 1997), 127–140.

[15] Lampariello, R., Agrawal, S., and Hirzinger, G.
Optimal motion planning for free-flying robots.
In *IEEE International Conference on Robotics and Automation*, Taipei, Taiwan, Sept. 2003, **3**, 3029–3035.

[16] Lampariello, R.
Motion planning for the on-orbit grasping of a non-cooperative target satellite with collision avoidance.
In *10th International Symposium on Artificial Intelligence, Robotics and Automation in Space*, Sapporo, Japan, 2010.

[17] Xu, W., Liang, B., Li, C., Liu, Y., and Xu, Y.
Autonomous target capturing of free-floating space robot: Theory and experiments.
Robotica, **27**, 3 (May 2009), 425–445.

[18] Dimitrov, D., and Yoshida, K.
Utilization of holonomic distribution control for reactionless path planning.
In *2006 IEEE/RSJ International Conference on Intelligent Robots and Systems*, Beijing, China, Oct. 2006, 3387–3392.

[19] Wang, H., and Xie, Y.
Prediction error based adaptive Jacobian tracking for free-floating space manipulators.
IEEE Transactions on Aerospace and Electronic Systems, **48**, 4 (Oct. 2012), 3207–3221.

[20] Dimitrov, D. N., and Yoshida, K.
Utilization of the bias momentum approach for capturing a tumbling satellite.
In *2004 IEEE/RSJ International Conference on Intelligent Robots and Systems*, Sendai, Japan, Sept.–Oct. 2004, **4**, 3333–3338.

[21] Dimitrov, D. N., and Yoshida, K.
Momentum distribution in a space manipulator for facilitating the post-impact control.
In *2004 IEEE/RSJ International Conference on Intelligent Robots and Systems*, Sendai, Japan, Sept.–Oct. 2004, **4**, 3345–3350.

[22] Yoshida, K., Dimitrov, D., and Nakanishi, H.
On the capture of tumbling satellite by a space robot.
In *2006 IEEE/RSJ International Conference on Intelligent Robots and Systems*, Beijing, China, Oct. 2006, 4127–4132.

[23] Oki, T., Nakanishi, H., and Yoshida, K.
Whole-body motion control for capturing a tumbling satellite target by a free-floating space robot.
In *IEEE/RSJ International Conference on Intelligent Robots and Systems*, San Diego, CA, Oct.–Nov. 2007, 2256–2261.

[24] Oki, T., Nakanishi, H., and Yoshida, K.
Time-optimal manipulator control for management of angular momentum distribution during the capture of a tumbling target.
Advanced Robotics, **24**, 3 (2010), 441–466.

[25] Oki, T., Abiko, S., Nakanishi, H., and Yoshida, K.
Time-optimal detumbling maneuver along an arbitrary arm motion during the capture of a target satellite.
In *2011 IEEE/RSJ International Conference on Intelligent Robots and Systems*, San Francisco, CA, Sept. 2011, 625–630.

[26] Aghili, F.
Optimal control of a space manipulator for detumbling a target satellite.
In *IEEE International Conference on Robotics and Automation*, Kobe, Japan, May 2009, 3019–3024.

[27] Aghili, F.
Coordination control of a free-flying manipulator and its base attitude to capture and detumble a noncooperative satellite.
In *IEEE/RSJ International Conference on Intelligent Robots and Systems*, St. Louis, MO, Oct. 2009, 2365–2372.

[28] Nguyen-Huynh, T. C., and Sharf, I.
Adaptive reactionless motion and parameter identification in

postcapture of space debris.
Journal of Guidance, Control, and Dynamics, **36**, 2 (2013), 404–414.

[29] Matsuno, F., and Saito, K.
Attitude control of a space robot with initial angular momentum.
In *IEEE International Conference on Robotics and Automation*, Seoul, Korea, May 2001, **2**, 1400–1405.

[30] Yamada, K., Yoshikawa, S., and Fujita, Y.
Arm path planning of a space robot with angular momentum.
Advanced Robotics, **9**, 6 (1994), 693–709.

[31] Nenchev, D., Umetani, Y., and Yoshida, K.
Analysis of a redundant free-flying spacecraft/manipulator system.
IEEE Transactions on Robotics and Automation, **8**, 1 (Feb. 1992), 1–6.

[32] Nanos, K., and Papadopoulos, E.
On Cartesian motions with singularities avoidance for free-floating space robots.
In *2012 IEEE International Conference on Robotics and Automation*, St. Paul, MN, May 2012, 5398–5403.

[33] Sideris, T. C.
Ordinary Differential Equations and Dynamical Systems.
Amsterdam: Atlantis Press, 2013.

Kostas Nanos received his diploma in chemical engineering from the National Technical University of Athens (NTUA) in 2001 and his M.Eng. degree from the Interdepartmental Program of Postgraduate Studies in Automation of the mechanical engineering department at NTUA in 2003. Currently, he is a Ph.D. degree candidate with the department of mechanical engineering at NTUA. His current research interests include robotics, space manipulators, path planning, model-based control, and modeling of dynamic systems.

He is a member of the Technical Chamber of Greece (TEE).

Evangelos Papadopoulos (S'83—M'91—SM'97) received his diploma from the National Technical University of Athens (NTUA) in 1981 and his M.S. and Ph.D. degrees from MIT in 1983 and 1991, respectively, all in mechanical engineering. He was an analyst with the Hellenic Navy, Athens, Greece, from 1985 to 1987. In 1991 he joined McGill University and the Centre for Intelligent Machines as an assistant professor. Currently, he is a professor with the department of mechanical engineering at the NTUA.

He teaches courses in the areas of systems, controls, mechatronics, and robotics. His research interests are in the areas of robotics, modeling and control of dynamic systems, mechatronics, and design. He serves as an associate editor for the *ASME Journal of Dynamic Systems, Measurement and Control* and *Machine and Mechanism Theory*, while previously he served as an associate editor of *IEEE Transactions on Robotics* and as a guest editor for *IEEE/ASME Transactions on Mechatronics*. He has published more than 200 technical articles in journals and refereed conference proceedings. He is a senior member of AIAA and a member of the ASME, the Technical Chamber of Greece, and Sigma Xi.